Chemical stability of Li_4PS_4I solid electrolyte against hydrolysis

Marcela Calpa[a], Nataly Carolina Rosero-Navarro[b*], Akira Miura[b], Randy Jalem[c,d,e], Yoshitaka Tateyama[c,e] and Kiyoharu Tadanaga[b]

[a.] Graduate School of Chemical Sciences and Engineering, Hokkaido University, Sapporo 060-8628, Japan

[b.] Division of Applied Chemistry, Faculty of Engineering, Hokkaido University, Sapporo 060-8628, Japan

[c.] Center for Green Research on Energy and Environmental Materials (GREEN), National Institute for Materials Science (NIMS), Tsukuba, Ibaraki 305-0044, Japan

[d.] PRESTO, Japan Science and Technology Agency (JST), Saitama 333-0012, Japan

[e.] Elements Strategy Initiative for Catalysts & Batteries, Kyoto University, Kyoto, Kyoto 615-8245, Japan

* corresponding author: rosero@eng.hokudai.ac.jp

Abstract

Sulfide solid electrolytes in the Li_3PS_4–LiI system are promising for all-solid-state batteries owing to their high ionic conductivity in the order of 10^{-4} S cm^{-1} and electrochemical stability. Nonetheless, the low chemical stability tendency of sulfide-based materials under ambient atmosphere is a critical issue due to the generation of toxic H_2S gas.

In this study, the chemical stability of Li_4PS_4I (Li_3PS_4–LiI) solid electrolyte under ambient atmosphere was investigated and compared with that of Li_3PS_4 to analyze the effect of the incorporation of LiI on the chemical stability of sulfide-based electrolytes.

No generation of H_2S gas was detected in the Li_4PS_4I solid electrolyte after an exposure of 60 min to the ambient atmosphere with high relative humidity of 40%. The hydrolysis suppression is attributed to the formation of $LiI{\cdot}H_2O$, acting as a protective barrier between PS_4^{3-} units in the electrolyte with H_2O molecules in air. The structural reversibility of Li_4PS_4I by simple drying at 180 °C was confirmed and the solid electrolyte exhibited an ionic conductivity of 10^{-4} S cm^{-1} at room temperature, similar to that of the sample before the exposure to the ambient atmosphere.

Keywords: Solid electrolyte, Sulfide electrolyte, Chemical stability, Lithium battery, All-solid-state battery

1. Introduction

Lithium batteries are promising candidates as the battery technology for applications such as electric vehicles and smart grids. However, Lithium-ion batteries (LIBs) using liquid electrolytes[1, 2] suffer from safety issues because of the risk of leakage and flammability. All-solid-state lithium batteries using inorganic solid electrolytes are expected to replace LIBs because of the improvement on the safety and their potential to achieve higher energy density[3, 4].

Among solid electrolytes, sulfide-based electrolytes have attracted significant attention due to their relatively high ionic conductivity[5, 6], and low Young's modulus[7], which is beneficial for producing favorable interface contacts with electrode materials by simple pressing at room temperature. However, the low chemical stability of sulfide-based electrolytes in the ambient atmosphere is a significant challenge. Conventional sulfide solid electrolytes can react with H_2O molecules in the air resulting in the generation of the toxic H_2S gas. Thus, it is necessary to use dry atmospheres for material preparation and battery assembly, which increases production costs and decreases the reliability of the batteries.

The chemical stability of sulfide solid electrolytes under the ambient atmosphere was first investigated by Tatsumisago et al.[8]. It was found that solid electrolytes formed by only PS_4^{3-} units were more stable, generating minimal amounts of H_2S upon exposure to the ambient atmosphere. The same group investigated the suppression of the generation of H_2S gas in Li_2S–P_2S_5 sulfide electrolytes using additives such as metal sulfide and metal oxides[9, 10]. Although it was effective in reducing the generation of H_2S gas, the ionic conductivity of the solid electrolytes was slightly decreased. Oxygen or nitrogen substitution in Li_2S–P_2S_5 electrolytes was also found to enhance their chemical stability in the ambient atmosphere [11, 12]. On the other hand, Liang et al.

investigated the replacement of P by Sn and As to improve the air stability of sulfide-based solid electrolytes, because according to the hard and soft acids and bases (HSAB) theory [13] Sn and As are less prone to react with oxygen than P. Although the reported $Li_{3.833}Sn_{0.833}As_{0.166}S_4$ exhibited higher air stability in comparison to Li_3PS_4, the toxic nature of As raises additional problems. Recently, Sun et al. used the same strategy to enhance the air stability of an argyrodite-type electrolyte by the partial substitution of P by Sn[14] and $Li_{10}GeP_2S_{12}$ by the partial substitution of P by Sb[15]. Compared to those without P substitution, these modified materials exhibited higher air stability at the exposure to dry room environments with humidity in the range of 1%–3%.

In this study, we investigate the effect of the incorporation of LiI on the chemical stability of sulfide solid electrolytes under the ambient atmosphere. The incorporation of LiI is effective in enhancing the ionic conductivity[16, 17] and electrochemical stability[18-21], and recent studies indicate that lithium halides have the potential to increase the stability against moisture[22, 23]. Here, the chemical stability of Li_4PS_4I (Li_3PS_4–LiI), whose structure is formed by PS_4^{3-} units and I^- ions[24], was investigated and compared to that of Li_3PS_4, whose structure is formed by PS_4^{3-} units only.

2. Experimental section

2.1 Synthesis

$Li_3PS_4 \cdot 2ACN$ was prepared by mixing Li_2S (Mitsuwa Chemical, 99.9%) and P_2S_5 (Aldrich, 99%) in a stoichiometric ratio of 3.0:1.3 (excess of P_2S_5 was used) in anhydrous acetonitrile (Wako Pure Chemical Industries) for 3 days using magnetic stirring. The obtained suspension was centrifuged at 10000 rpm for 10 min and

decanted to recover solid powders. The solid powders were subsequently dried under vacuum at 80 °C for 3 h to remove excess of solvent and to obtain Li_3PS_4·2ACN [25], as confirmed by X-ray diffraction (Figure S1). The Li_3PS_4 sample was prepared by heating Li_3PS_4·2ACN at 220 °C for 1 h.

Li_3PS_4·xLiI solid electrolytes were prepared by mixing Li_3PS_4·2ACN and LiI (Sigma Aldrich, 99.9%) in molar compositions of x = 0.5, 1 and 1.5, in anhydrous acetonitrile (Wako Pure Chemical Industries) for 15 min. Each mixture was dried under vacuum at 100 °C for 3 h using a rotary evaporator (Eyela N-1300), to remove the solvent and to obtain solid powders. Subsequently, each sample was heated at 220 °C for 1 h.

2.2 Characterization

The structure of the solid electrolytes, after heat treatment at 220 °C, was studied by XRD and Raman spectroscopy. To identify the crystalline phases of the samples, XRD measurements were performed using an X-ray diffractometer (Miniflex 600, Rigaku) using CuKα radiation. Diffraction data were collected in steps of 0.01 in the range of 10°–40° in 2θ. Indexation of XRD patterns was performed using Rigaku PDXL software. To identify the structural units of the samples, Raman spectroscopy was performed using a Raman spectrometer (HORIBA XploRA PLUS Scientific). The Raman shift was in the range of 300 cm^{-1}–3000 cm^{-1}.

The ionic conductivity of pelletized samples was analyzed by electrochemical impedance spectroscopy (EIS). The solid electrolyte powders (30 mg) were pressed at around 360 MPa (at room temperature) in a polycarbonate tube with a diameter of 6 mm, and two stainless steel disks were used as current collectors. The EIS measurements were conducted using an impedance analyzer (SI 1260, Solartron) in

the frequency range of 0.1 MHz to 1 Hz at an amplitude of 10 mV. All processes were performed under an argon atmosphere.

The chemical stability of the solid electrolytes in the ambient atmosphere was monitored by measuring the H_2S gas generation and by X-ray diffraction. The powder samples (~15 mg) were first pressed at 25 MPa for convenient handling. Each pelletized sample and an H_2S gas sensor (ToxiRAE Pro PGM-1860) were placed in a closed 2000 cm^3 desiccator in air. The air temperature was 20 °C, and the relative humidity was 40%. The H_2S concentration was measured by a gas sensor with a resolution of 1 ppm, and automatically recorded at 30-s intervals. The amount of H_2S gas generated from the samples was calculated from the H_2S concentration.

Following exposure to the ambient atmosphere for 60 or 1800 min, each sample was kept under an Argon atmosphere. Prior to the XRD measurements, the air-exposed samples were ground using an Agatha mortar.

Selected samples were also examined by Scanning Electron Microscopy (SEM) coupled with Energy Dispersive X-ray Spectroscopy (EDX, TM3030Plus Miniscope, Hitachi), before and after exposure to the ambient atmosphere.

2.3 Computational details

Reaction energies related to the hydrolysis of Li_3PS_4 and Li_4PS_4I were calculated by DFT (Density Functional Theory) using candidate competing phases from the Materials Project[26, 27]. Additional phases not included in the latter were taken from ICSD and were separately calculated by DFT (using the VASP code[23,24]) to determine their total energies. Energy correction schemes, as implemented in the Materials Project, were also performed as needed. For the Li_3PS_4 and Li_4PS_4I[19] electrolyte compounds, the *Pnma* and *P*4/*nmm* (origin choice 2) symmetry were adopted,

respectively. The former has full Li-site occupancy while the latter has partial occupancy in 5 Wyckoff sites (2*c*, 2*a*, 8*j*, 4*d*, and 8*i*). For geometry optimization, the following conditions were employed: 520-eV kinetic energy cutoff, switched-on spin polarization, and at least 1000-kpoint resolution (Monkhorst-Pack grid[25]). Standard pseudopotentials were used for the various elements, except for Li in which the potential used has semicore *s* states treated as valence states. Calculations were confirmed to converge to within 1 meV/atom and 0.01 eV/Å in energy and residual forces, respectively.

About 10 random configurations for the Li-vacancy arrangement were geometry-optimized by DFT for Li_4PS_4I in a model described by supercell vectors (1, 1, 0), (-1, 1, 0), and (0, 0, 2), leading to a structure with 80 atoms and at least 12-Å in cell edges. The lowest-energy structure was then chosen for subsequent calculations, such as reaction energy calculations and as initial structure to generate the proton-incorporated model (i.e., Li^+/H^+ exchange). Another set of 10 structures with randomly sampled Li-H configurations were geometry-optimized as well, with the total energy of the lowest-energy structure used for reaction energy calculations.

In the case Li_3PS_4, a model (120 atoms with at least 12-Å in cell edges) described by supercell vectors (2, 0, 0), (0, 2, 0), and (0, 0, 1) was created. Similar to Li_4PS_4I, 10 structures with randomly generated Li-H configurations were also sampled, with the total energy of the lowest-energy structure was used for calculating reaction energies.

3. Results and discussion

To investigate the formation of the Li_4PS_4I crystal phase, $Li_3PS_4 \cdot xLiI$ solid electrolytes with x=0, 0.5, 1 and 1.5, were investigated by X-ray diffraction, Raman spectroscopy, and EIS.

Figure 1a shows the X-ray diffraction (XRD) patterns of the synthesized Li_3PS_4·xLiI solid electrolytes. The XRD patterns of β-Li_3PS_4 (ICSD#180318), Li_4PS_4I (Chem. Mater., 29 (2017), p. 1830[24]) and LiI (ICSD#414244) crystal phases are shown for comparison. The XRD pattern of the sample without addition of LiI (x=0), exhibited the formation of the β-Li_3PS_4 crystal phase. The XRD pattern of the sample with x = 0.5 shows peaks corresponding to the Li_4PS_4I crystal phase in addition to β-Li_3PS_4. The XRD pattern of the sample with x = 1 shows peaks corresponding to the Li_4PS_4I crystal phase [24] only. The XRD pattern of the sample with x = 1.5 shows peaks corresponding to LiI in addition to the Li_4PS_4I crystal phase. Indexed XRD patterns of samples with x = 0 and 1 are shown in Figure S2 and Figure S3, respectively.

Figure 1b shows the Raman spectra of the Li_3PS_4·xLiI solid electrolytes corresponding to the same conditions as those in of the XRD study (Figure 1a). The sample without the addition of LiI exhibited a band centered at 421 cm^{-1}. The sample with x = 0.5 also exhibited a band centered at 421 cm^{-1}, however wider. The sample with x = 1 exhibited a band centered around 417 cm^{-1} and the sample with x = 1.5 exhibited a band centered at 425 cm^{-1}.

The Raman band centered at 421 cm^{-1} in the sample without the addition of LiI is attributed to the symmetric stretching of the P–S bonds in the PS_4^{3-} units[28], which form the local structure of the β-Li_3PS_4 crystal structure. The Raman band of the sample with x = 1 centered at 417 cm^{-1} is attributed to the PS_4^{3-} units in the Li_4PS_4I crystal structure. The slight change in the Raman shift of the sample with x = 1 is attributed to the change in the local environment of the PS_4^{3-} units due to the incorporation of LiI.

Figure 2 shows the temperature dependence of the ionic conductivity of the Li_3PS_4·xLiI solid electrolytes. The Li_3PS_4·xLiI samples attained ionic conductivities of 0.5 × 10^{-4},

1.5×10^{-4}, 1.3×10^{-4} and 0.9×10^{-4} S cm^{-1} at room temperature, and activation energy of 9.78, 12.04 and 12.04, and 19.31 kJ mol^{-1} for x=0, 0.5, 1 and 1.5, respectively (Table S4).

The Li_4PS_4I crystal phase is formally obtained from Li_3PS_4 and LiI in 1:1 molar ratio. However, the analysis of the $Li_3PS_4 \cdot xLiI$ samples by XRD, Raman spectroscopy, and EIS indicated that the Li_4PS_4I crystal phase also nucleated at compositions with lower LiI contents. As confirmed, the local structure of the $Li_3PS_4 \cdot xLiI$ samples was formed by PS_4^{3-} units, separated by I^- ions according to the x content. The ionic conductivity of the samples containing the Li_4PS_4I crystal phase ($1.3–1.5 \times 10^{-4}$ S cm^{-1}) was slightly higher than that reported by Sedlmaier et al. ($0.64–1.2 \times 10^{-4}$ S cm^{-1}) [24]. It is worth noting that even higher ionic conductivity in Li_2S-P_2S_5-LiI solid electrolytes prepared by liquid-phase can be achieved by optimizing the synthesis conditions[29, 30]. A LiI content higher than x = 1 was not incorporated, which resulted in a decrease in the ionic conductivity.

To investigate the effect of the incorporation of LiI on the stability of sulfide-based solid electrolytes under ambient atmosphere, the generation of H_2S gas from Li_4PS_4I (x = 1) due to exposure to the ambient atmosphere was measured and compared to that of Li_3PS_4 (x = 0).

Figures 3a and b show the amount of H_2S gas generated from the pelletized Li_3PS_4 and Li_4PS_4I samples during 60 min (Figure 3a) and up to 1800 min (Figure 3b) of exposure to the ambient atmosphere. The temperature was 20 °C, and the relative humidity was 40%.

After an exposure of 60 min to the ambient atmosphere (Figure 3a), the amount of H_2S generated from the Li_3PS_4 sample was 0.82 cm^3 g^{-1}. The amount of H_2S

generated from the Li_4PS_4I sample was below the lower detection limit of the H_2S gas sensor (1 ppm).

After approximately 540 min (Figure 3b), the H_2S gas generation from the Li_3PS_4 and Li_4PS_4I samples reached maximum values of 8.3 and 0.96 $cm^3\ g^{-1}$, respectively. The detection of the H_2S gas stabilized at the maximum peak for a certain time and subsequently decreased in both cases. It is believed that the H_2S gas could undergo certain reaction in air[31], which would prevent the further detection of the H_2S gas generation.

Figure 3c shows images of the Li_3PS_4 and Li_4PS_4I samples after exposure to the ambient atmosphere for 1800 min. The Li_3PS_4 sample pellet completely disintegrated, which is attributed to the decomposition that the sample suffered due to the long exposure to the ambient atmosphere with high relative humidity (40 %). Nevertheless, the Li_4PS_4I sample pellet did not exhibit significant change despite the generation of a small amount of H_2S gas.

To understand the mechanism of H_2S gas suppression in the Li_4PS_4I sample, the crystal structure of the Li_3PS_4 and Li_4PS_4I samples was investigated after the exposure to the ambient atmosphere. Figure 4a shows the XRD patterns of the Li_3PS_4 sample after exposure to the ambient atmosphere for 60 and 1800 min. The XRD pattern of the pristine sample and β-Li_3PS_4 (ICSD#180318) are shown for comparison. Prior to exposure to the ambient atmosphere, XRD peaks corresponding to the β-Li_3PS_4 crystal phase were observed, as discussed above. After 60 min of air exposure, unknown XRD peaks were observed in addition to those corresponding to the β-Li_3PS_4 crystal phase. After 1800 min, additional unknown XRD peaks were observed. The unknown XRD peaks can be attributed to the products of the reactions between the PS_4^{3-} units and the H_2O molecules in the air due to the long exposure to the ambient

atmosphere. Although structural changes were clearly observed by X-ray diffraction, no significant changes were observed by Raman spectroscopy (Figure S8), and similar results were reported by Tatsumisago et al. [5].

Figure 4b shows the XRD patterns of the Li_4PS_4I sample after exposure to the ambient atmosphere for 60 and 1800 min. The XRD pattern of the pristine sample, Li_4PS_4I (Chem. Mater., 29 (2017), p. 1830[24]), $LiI{\cdot}H_2O$ (ICSD #25515) and $LiI{\cdot}3H_2O$ (ICSD #759794) are shown for comparison.

Prior to the exposure to the ambient atmosphere, XRD peaks corresponding to the Li_4PS_4I crystal phase were observed, as discussed above. After 60 min of air exposure, additional XRD peaks corresponding to $LiI{\cdot}H_2O$[32] and minor unknown XRD peaks were observed. After 1800 min, XRD peaks corresponding to $LiI{\cdot}3H_2O$ and unknown XRD peaks were observed.

The unknown XRD peaks attributed to the decomposition of the PS_4^{3-} units observed in the XRD pattern of the Li_3PS_4 sample after exposure to the ambient atmosphere for 60 min were not observed in the XRD pattern of the Li_4PS_4I sample, which confirmed that the PS_4^{3-} units in the Li_4PS_4I sample did not undergo decomposition. The XRD pattern of the Li_4PS_4I sample after exposure to the ambient atmosphere for 60 min also revealed the formation of $LiI{\cdot}H_2O$. The presence of unknown peaks in the XRD pattern of the Li_4PS_4I sample after exposure to the ambient atmosphere for 1800 min revealed that the sample underwent certain decomposition; however, it was minor in comparison to that of the Li_3PS_4 sample, as observed by the H_2S gas generation (Figure 3b).

Figure 5 illustrates the energy level of the reactions of Li_4PS_4I and Li_3PS_4 towards water gas calculated by DFT. Reaction 1 relates to the formation of $LiI{\cdot}H_2O$ observed experimentally in the Li_4PS_4I sample when exposed to moisture:

$Li_4PS_4I + H_2O \rightarrow Li_3PS_4 + LiI{\cdot}H_2O$, ΔH (cal) =−0.19 eV (1)

When in contact with H_2O, Li_4PS_4I is determined to have $\Delta H < 0$ for the formation of $LiI{\cdot}H_2O$, in agreement with the experimental results (Figure 4b).

Reaction 2 relates to the hydrolysis of Li_3PS_4:

$Li_3PS_4 + 4H_2O \rightarrow Li_3PO_4 + 4H_2S$, ΔH (cal) =−0.96 eV (2)

When in contact with H_2O, Li_3PS_4 is determined to have $\Delta H < 0$ for the formation of H_2S, which indicates that this reaction is thermodynamically favorable. It explains the H_2S gas generation from the Li_3PS_4 sample at the exposure to moisture in the ambient atmosphere (Figure 3). Unknown peaks observed in the XRD patterns of the Li_3PS_4 sample after exposure to the ambient atmosphere (Figure 4a) may be assigned to the decomposition products of Li_3PO_4 (Reactions s1 and s2, supporting information).

Based on the above experimental and theoretical results, the hydrolysis stability of Li_4PS_4I is attributed to kinetic rather than thermodynamic origin. From the viewpoint of physical stability, $LiI{\cdot}H_2O$ should result into an effective barrier between PS_4^{3-} units in Li_4PS_4I electrolyte and H_2O in air.

The formation of $LiI{\cdot}H_2O$ as a protective barrier was further investigated by SEM. Figure 6 shows an SEM image and corresponding EDX elemental mappings for Phosphorus (P), Sulfur (S), and Iodine (I) of the Li_4PS_4I sample (pressed at low pressure to facilitate handling, see experimental section) prior to exposure to the ambient atmosphere. The EDX elemental mappings showed a homogeneous distribution of P, S, and I in the Li_4PS_4I sample.

Figure 7a shows an SEM image of the Li_4PS_4I sample after exposure to the ambient atmosphere for 60 min. The formation of a layer covering the surface of the sample was observed, and the corresponding EDX elemental analysis indicated a rich iodine ratio (iodine/phosphorus ratio=2.2), higher than that in the pristine Li_4PS_4I

(iodine/phosphorus ratio=1). Figures 7b-f show higher magnification of the selected area in Figure 7a (white box) and corresponding EDX elemental mappings for Phosphorus (P), Sulfur (S), Iodine (I), and Oxygen (O). The EDX elemental mapping indicated that oxygen (Figure 7f) was mainly located on the covering layer. These results suggest that $LiI{\cdot}H_2O$, observed by XRD (Figure 4b), is formed after exposure to the ambient atmosphere, acting as a protective layer and preventing the direct contact between the sample and H_2O molecules in the air.

It is worth noting that similar results were found by Goodenough et al. The introduction of the Lithium halide LiF to the garnet $Li_{6.5}La_3Zr_{1.5}Ta_{0.5}O_{12}$, increased the stability of the garnet electrolyte against moist air. The enhanced stability was attributed to LiF in the grain boundary of the garnet preventing the diffusion of moisture into the pellet. The results found by Goodenough et al.[22, 33], and in this work opens a new alternative for improving the stability of solid electrolytes in the ambient atmosphere by the introduction of lithium halides.

The dehydration of the Li_4PS_4I sample after being exposed to the ambient atmosphere, by simple drying at 180 °C under vacuum for 4 h, was investigated by XRD and Raman spectroscopy.

Figure 8a shows the XRD pattern of the Li_4PS_4I sample after exposure to the ambient atmosphere for 60 min and subsequent drying at 180 °C. The XRD patterns of the Li_4PS_4I sample before and after exposure to the ambient atmosphere are shown for comparison. After drying at 180 °C, only the XRD peaks corresponding to the Li_4PS_4I crystal phase were observed

Figure 8b shows the Raman spectrum of the Li_4PS_4I sample after exposure to the ambient atmosphere and subsequent drying at 180 °C. The Raman spectra of the Li_4PS_4I sample prior to and after the exposure to the ambient atmosphere are shown

for comparison. The Raman spectrum of the sample after the exposure to the ambient atmosphere exhibited a band centered at 415 cm^{-1}. The slight shift in comparison to the band observed prior to the exposure to the ambient atmosphere (417 cm^{-1}) can be attributed to the change in the local environment due to the formation of $LiI{\cdot}H_2O$. Nevertheless, the Raman spectrum after drying the sample at 180 °C exhibited a band centered at 417 cm^{-1}, similar to the Raman band observed prior exposure to the ambient atmosphere.

The reversibility of the Li_4PS_4I crystal phase by simple drying was confirmed by XRD and Raman spectroscopy. Moreover, the Li_4PS_4I sample after exposure to the ambient atmosphere and subsequent drying at 180 °C under vacuum, exhibited an ionic conductivity of 0.7×10^{-4} S cm^{-1} at room temperature (19 °C), similar to that of the sample prior to the exposure to the ambient atmosphere.

4. Conclusion

The formation of the Li_4PS_4I crystal phase in $Li_3PS_4{\cdot}xLiI$ solid electrolytes with x=0.5, 1 and 1.5, was investigated by XRD, Raman spectroscopy, and EIS. The Li_4PS_4I crystal phase was found to nucleate with LiI incorporation of x = 1 or lower. A higher LiI content of x = 1.5 was not completely incorporated. As confirmed, the local structure of the $Li_3PS_4{\cdot}xLiI$ samples was formed by PS_4^{3-} units, separated by I^- ions, according to the LiI incorporation. Solid electrolytes containing Li_4PS_4I crystal phase exhibited an ionic conductivity of $1.3–1.5 \times 10^{-4}$ S cm^{-1}.

The chemical stability of the Li_4PS_4I sample (x = 1) in the ambient atmosphere was investigated and compared to that of Li_3PS_4 (x = 0), by measuring the H_2S gas generation, to analyze the effect of the incorporation of LiI on the chemical stability in the ambient atmosphere of sulfide-based electrolytes. No generation of H_2S gas was detected in the Li_4PS_4I solid electrolyte after 60 min of exposure to the ambient

atmosphere. The suppression of hydrolysis is attributed to the formation of $LiI{\cdot}H_2O$, acting as a protective barrier and preventing the direct contact between PS_4^{3-} units in the bulk electrolyte with H_2O molecules in air.

Acknowledgments

This research was partly supported by the SOLiD-EV Project of the New Energy and Industrial Technology Development Organization (NEDO), Japan. R. Jalem and Y. Tateyama are grateful for financial supports by JSPS KAKENHI Grant Number JP19H05815, and by MEXT as "Program for Promoting Researches on the Supercomputer Fugaku (Fugaku Battery & Fuel Cell Project), Grant Number JPMXP1020200301 and Materials Processing Science project ("Materealize"), Grant Number JPMXP0219207397. Calculations were carried out on the supercomputer at NIMS.

References

1. Weiss, M.; Simon, F. J.; Busche, M. R.; Nakamura, T.; Schröder, D.; Richter, F. H.; Janek, J., From Liquid-to Solid-State Batteries: Ion Transfer Kinetics of Heteroionic Interfaces. *Electrochemical Energy Reviews* **2020**, 1-18.

2. Chu, Y.; Shen, Y.; Guo, F.; Zhao, X.; Dong, Q.; Zhang, Q.; Li, W.; Chen, H.; Luo, Z.; Chen, L., Advanced characterizations of solid electrolyte interphases in lithium-ion batteries. *Electrochemical Energy Reviews* **2020,** 3, (1), 187-219.

3. Oh, G.; Hirayama, M.; Kwon, O.; Suzuki, K.; Kanno, R., Bulk-type all solid-state batteries with 5V class $LiNi_{0.5}Mn_{1.5}O_4$ cathode and $Li_{10}GeP_2S_{12}$ solid electrolyte. *Chemistry of Materials* **2016,** 28, (8), 2634-2640.

4. Sun, C.; Liu, J.; Gong, Y.; Wilkinson, D. P.; Zhang, J., Recent advances in all-solid-state rechargeable lithium batteries. *Nano Energy* **2017,** 33, 363-386.

5. Kamaya, N.; Homma, K.; Yamakawa, Y.; Hirayama, M.; Kanno, R.; Yonemura, M.; Kamiyama, T.; Kato, Y.; Hama, S.; Kawamoto, K., A lithium superionic conductor. *Nature materials* **2011,** 10, (9), 682.

6. Kato, Y.; Hori, S.; Saito, T.; Suzuki, K.; Hirayama, M.; Mitsui, A.; Yonemura, M.; Iba, H.; Kanno, R., High-power all-solid-state batteries using sulfide superionic conductors. *Nature Energy* **2016,** 1, (4), 16030.

7. Sakuda, A.; Hayashi, A.; Tatsumisago, M., Sulfide solid electrolyte with favorable mechanical property for all-solid-state lithium battery. *Scientific reports* **2013,** 3, 2261.

8. Muramatsu, H.; Hayashi, A.; Ohtomo, T.; Hama, S.; Tatsumisago, M., Structural change of Li_2S–P_2S_5 sulfide solid electrolytes in the atmosphere. *Solid State Ionics* **2011,** 182, (1), 116-119.

9. Ohtomo, T.; Hayashi, A.; Tatsumisago, M.; Kawamoto, K., Suppression of H_2S gas generation from the $75Li_2S{\cdot}25P_2S_5$ glass electrolyte by additives. *Journal of Materials Science* **2013,** 48, (11), 4137-4142.

10. Hayashi, A.; Muramatsu, H.; Ohtomo, T.; Hama, S.; Tatsumisago, M., Improvement of chemical stability of Li_3PS_4 glass electrolytes by adding M_xO_y (M= Fe, Zn, and Bi) nanoparticles. *Journal of Materials Chemistry A* **2013,** 1, (21), 6320-6326.

11. Fukushima, A.; Hayashi, A.; Yamamura, H.; Tatsumisago, M., Mechanochemical synthesis of high lithium ion conducting solid electrolytes in a Li_2S-P_2S_5-Li_3N system. *Solid State Ionics* **2017,** 304, 85-89.

12. Ohtomo, T.; Hayashi, A.; Tatsumisago, M.; Kawamoto, K., Characteristics of the Li_2O–Li_2S–P_2S_5 glasses synthesized by the two-step mechanical milling. *Journal of non-crystalline solids* **2013,** 364, 57-61.

13. Sahu, G.; Lin, Z.; Li, J.; Liu, Z.; Dudney, N.; Liang, C., Air-stable, high-conduction solid electrolytes of arsenic-substituted Li_4SnS_4. *Energy & Environmental Science* **2014,** 7, (3), 1053-1058.

14. Zhao, F.; Liang, J.; Yu, C.; Sun, Q.; Li, X.; Adair, K.; Wang, C.; Zhao, Y.; Zhang, S.; Li, W., A Versatile Sn-Substituted Argyrodite Sulfide Electrolyte for All-Solid-State Li Metal Batteries. *Advanced Energy Materials* **2020,** 10, (9), 1903422.

15. Liang, J.; Chen, N.; Li, X.; Li, X.; Adair, K. R.; Li, J.; Wang, C.; Yu, C.; Norouzi Banis, M.; Zhang, L., $Li_{10}Ge\ (P_{1-x}Sb_x)_2S_{12}$ Lithium-Ion Conductors with Enhanced Atmospheric Stability. *Chemistry of Materials* **2020,** 32, (6), 2664-2672.

16. Malugani, J.; Robert, G., Preparation and electrical properties of the $0{,}37Li_2S$-$0{,}18P_2S_5$-0,45LiI glass. *Solid State Ionics* **1980,** 1, (5-6), 519-523.

17. Mercier, R.; Malugani, J.-P.; Fahys, B.; Robert, G., Superionic conduction in Li_2S-P_2S_5-LiI-glasses. *Solid State Ionics* **1981,** 5, 663-666.

18. Ujiie, S.; Hayashi, A.; Tatsumisago, M., Structure, ionic conductivity and electrochemical stability of Li_2S–P_2S_5–LiI glass and glass–ceramic electrolytes. *Solid State Ionics* **2012,** 211, 42-45.

19. Ujiie, S.; Hayashi, A.; Tatsumisago, M., Preparation and ionic conductivity of (100− x)(0.8 Li_2S·0.2P_2S_5)· xLiI glass–ceramic electrolytes. *Journal of Solid State Electrochemistry* **2013,** 17, (3), 675-680.

20. Rangasamy, E.; Liu, Z.; Gobet, M.; Pilar, K.; Sahu, G.; Zhou, W.; Wu, H.; Greenbaum, S.; Liang, C., An iodide-based $Li_7P_2S_8I$ superionic conductor. *Journal of the American Chemical Society* **2015,** 137, (4), 1384-1387.

21. Han, F.; Yue, J.; Zhu, X.; Wang, C., Suppressing Li dendrite formation in Li_2S-P_2S_5 solid electrolyte by LiI incorporation. *Advanced Energy Materials* **2018,** 8, (18), 1703644.

22. Li, Y.; Xu, B.; Xu, H.; Duan, H.; Lü, X.; Xin, S.; Zhou, W.; Xue, L.; Fu, G.; Manthiram, A., Hybrid polymer/garnet electrolyte with a small interfacial resistance for lithium-ion batteries. *Angewandte Chemie International Edition* **2017,** 56, (3), 753-756.

23. Huang, J.; Liang, F.; Hou, M.; Zhang, Y.; Chen, K.; Xue, D., Garnet-type solid-state electrolytes and interfaces in all-solid-state lithium batteries: progress and perspective. *Applied Materials Today* **2020,** 20, 100750.

24. Sedlmaier, S. J.; Indris, S.; Dietrich, C.; Yavuz, M.; Dräger, C.; von Seggern, F.; Sommer, H.; Janek, J. r., Li_4PS_4I: a Li^+ superionic conductor synthesized by a solvent-based soft chemistry approach. *Chemistry of Materials* **2017,** 29, (4), 1830-1835.

25. Wang, H.; Hood, Z. D.; Xia, Y. N.; Liang, C. D., Fabrication of ultrathin solid electrolyte membranes of β-Li_3PS_4 nanoflakes by evaporation-induced self-assembly for all-solid-state batteries. *Journal of Materials Chemistry A* **2016,** 4, (21), 8091-8096.

26. Jain, A.; Ong, S. P.; Hautier, G.; Chen, W.; Richards, W. D.; Dacek, S.; Cholia, S.; Gunter, D.; Skinner, D.; Ceder, G., Commentary: The Materials Project: A materials genome approach to accelerating materials innovation. *Apl Materials* **2013,** 1, (1), 011002.

27. Ong, S. P.; Richards, W. D.; Jain, A.; Hautier, G.; Kocher, M.; Cholia, S.; Gunter, D.; Chevrier, V. L.; Persson, K. A.; Ceder, G., Python Materials Genomics (pymatgen): A robust, open-source python library for materials analysis. *Computational Materials Science* **2013,** 68, 314-319.

28. Tachez, M.; Malugani, J.-P.; Mercier, R.; Robert, G., Ionic conductivity of and phase transition in lithium thiophosphate Li_3PS_4. *Solid State Ionics* **1984,** 14, (3), 181-185.

29. Hikima, K.; Yamamoto, T.; Phuc, N. H. H.; Matsuda, R.; Muto, H.; Matsuda, A., Improved ionic conductivity of Li_2S-P_2S_5-LiI solid electrolytes synthesized by liquid-phase synthesis. *Solid State Ionics* **2020,** 354, 115403.

30. Indrawan, R. F.; Yamamoto, T.; Nguyen, H. H. P.; Muto, H.; Matsuda, A., Liquid-phase synthesis of $100Li_3PS_4$-50LiI-xLi_3PO_4 solid electrolytes. *Solid State Ionics* **2020,** 345, 115184.

31. Hales, J.; Wilkes, J.; York, J., Some recent measurements of H_2S oxidation rates and their implications to atmospheric chemistry 1. *Tellus* **1974,** 26, (1-2), 277-283.

32. Weiss, E., Die Kristallstruktur des Lithiumjodid-Monohydrats. *Zeitschrift für anorganische und allgemeine Chemie* **1965,** 341, (3-4), 203-206.

33. Xu, L.; Li, J.; Deng, W.; Shuai, H.; Li, S.; Xu, Z.; Li, J.; Hou, H.; Peng, H.; Zou, G., Garnet Solid Electrolyte for Advanced All-Solid-State Li Batteries. *Advanced Energy Materials* **2020**, 2000648.

FIGURES

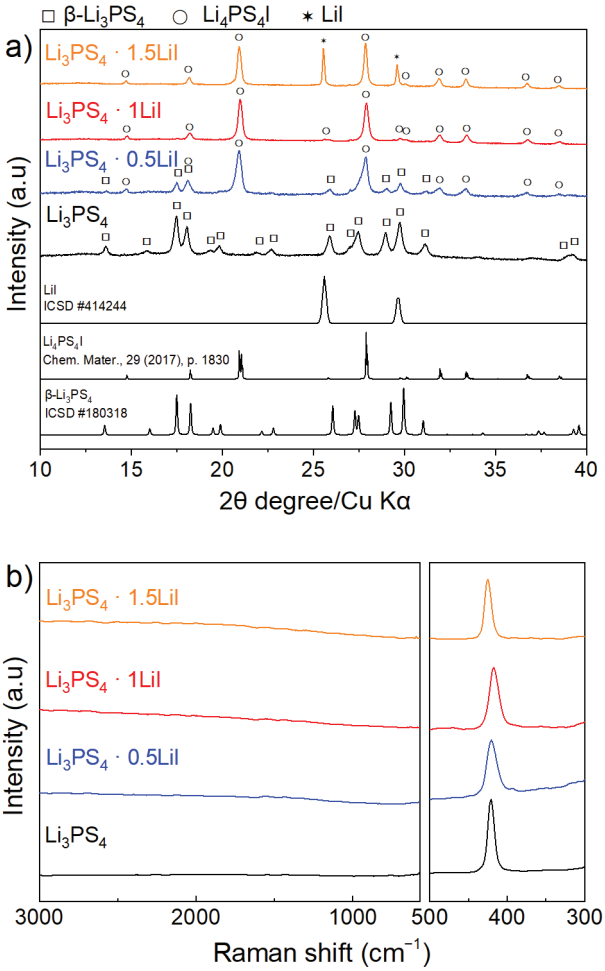

Figure 1 a) XRD patterns and b) Raman spectra of $Li_3PS_4 \cdot xLiI$ samples with x=0, 0.5, 1 and 1.5

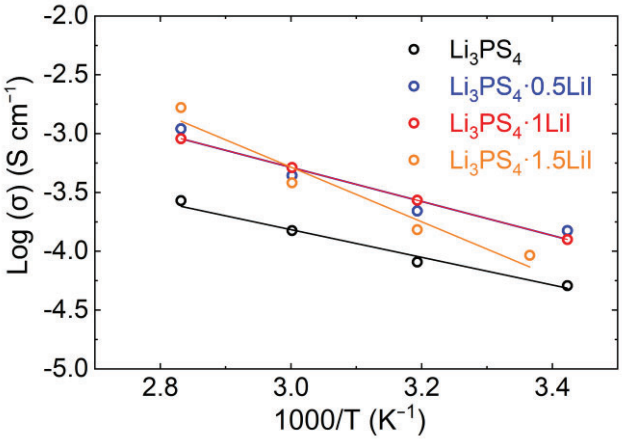

Figure 2. Arrhenius plot of $Li_3PS_4 \cdot xLiI$ samples with x=0, 0.5, 1 and 1.5

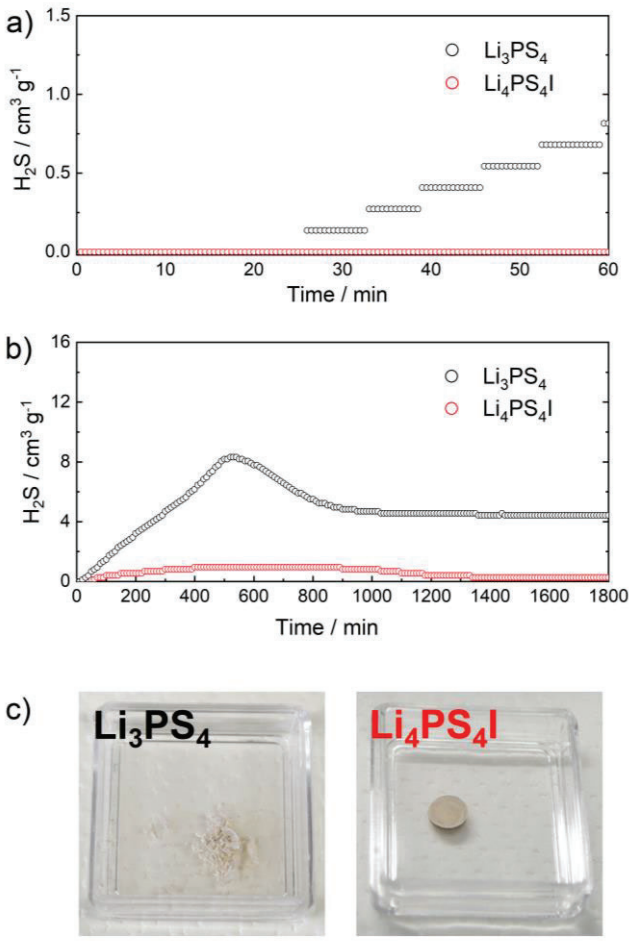

Figure 3. H_2S gas generation from Li_3PS_4 and Li_4PS_4I solid electrolytes a) during 60 min and b) up to 1800 min of exposure to the ambient atmosphere. The temperature was 20 °C, and the relative humidity was 40%. c) Photographs of the Li_3PS_4 and Li_4PS_4I samples after exposure to the ambient atmosphere for 1800 min.

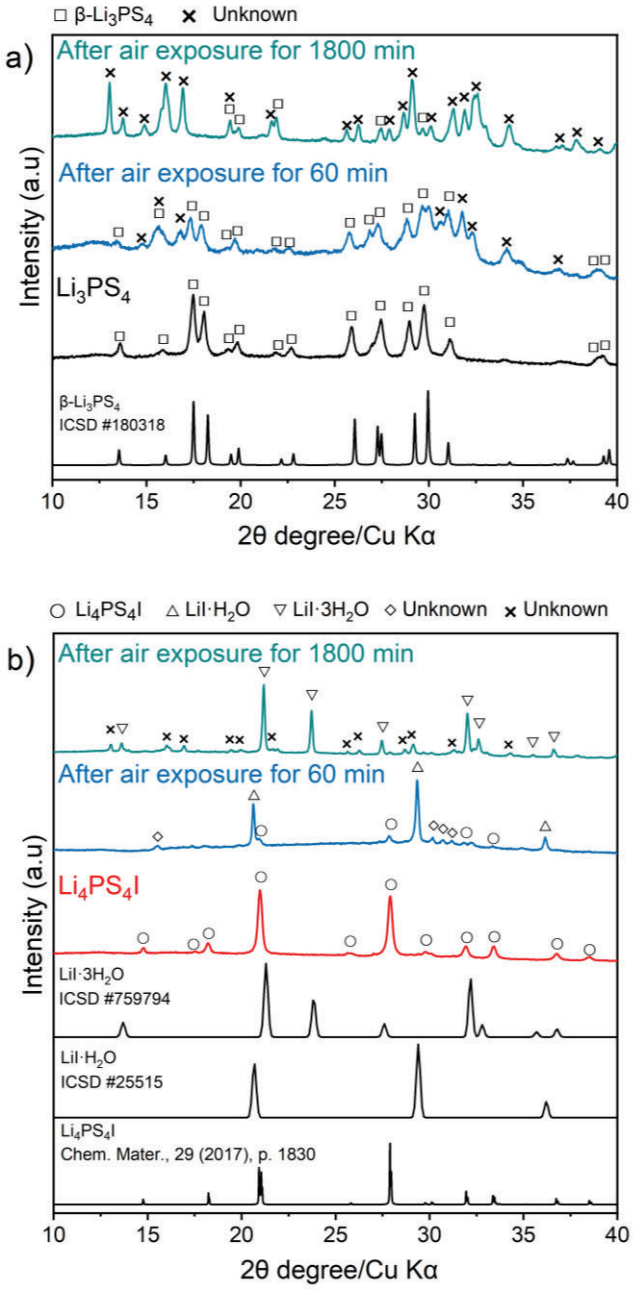

Figure 4. XRD patterns of a) Li_3PS_4 and b) Li_4PS_4I solid electrolytes prior to and after exposure to the ambient atmosphere for 60 min and 1800 min.

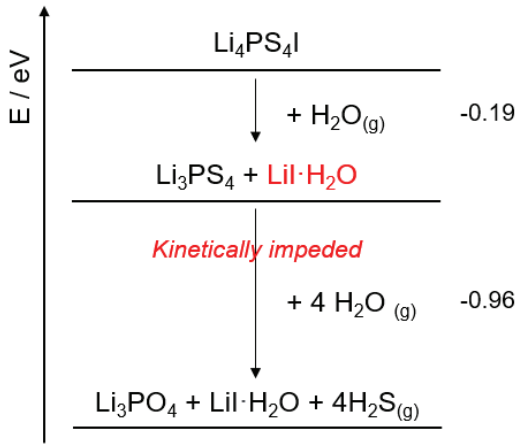

Figure 5. DFT-calculated energy (at 0 K) pertaining to the reaction between Li_4PS_4I and Li_3PS_4 with H_2O.

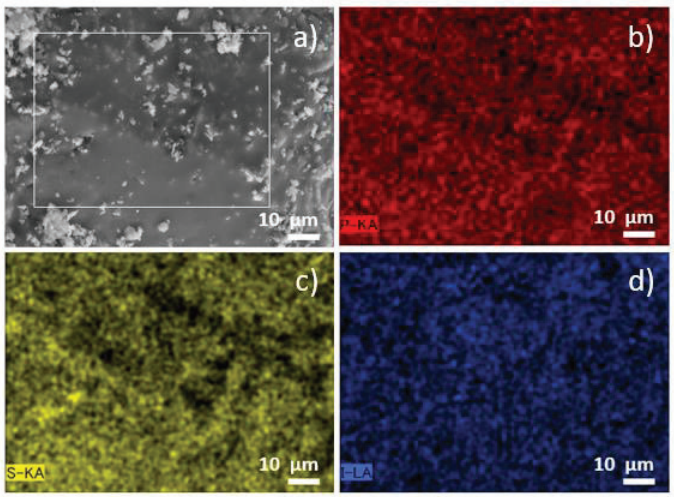

Figure 6 a) SEM image of the Li_4PS_4I sample prior exposure to the ambient atmosphere, and corresponding EDX elemental mapping of selected area (white box) for Phosphorus (b), Sulfur (c), and Iodine (d).

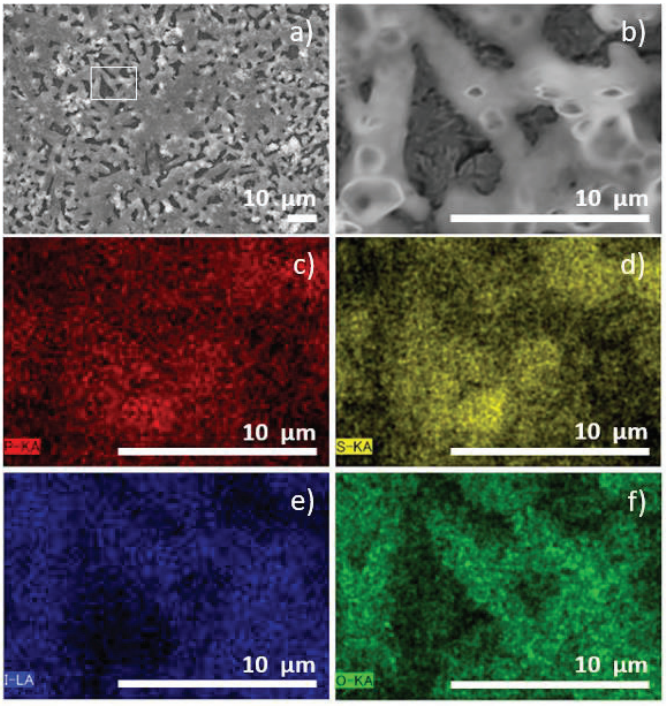

Figure 7 a) SEM image of the Li_4PS_4I sample after exposure to the ambient atmosphere for 60 min. b) Higher magnification of selected area in a) (white box), and c-f) corresponding EDX elemental mapping for Phosphorus (c), Sulfur (d) Iodine (e) and oxygen (f).

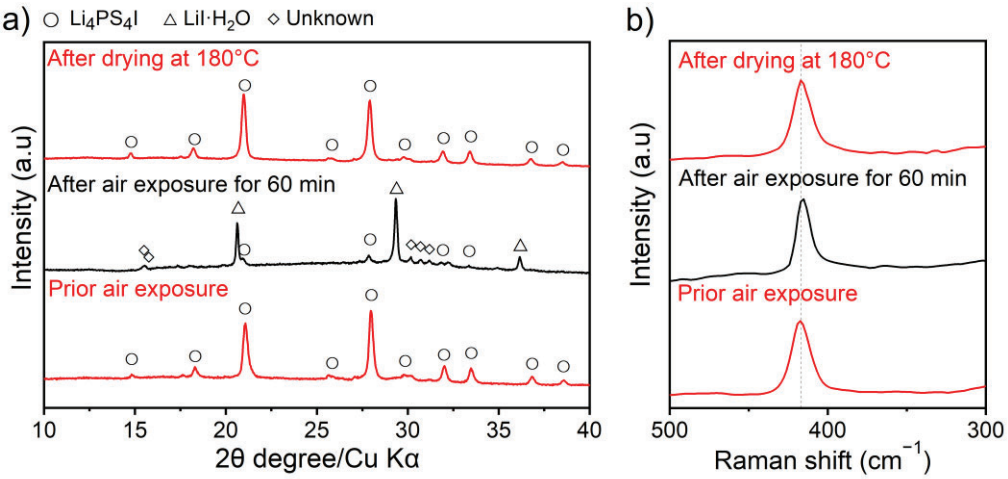

Figure 8. a) XRD pattern and b) Raman spectra of the Li_4PS_4I solid electrolyte, prior exposure to the ambient atmosphere, after exposure to the ambient atmosphere for 60 min and after subsequently drying at 180 °C.